*universe*

MDPI

*Article*

# Null and Timelike Geodesics near the Throats of Phantom Scalar Field Wormholes †

**Ivan Potashov, Julia Tchemarina and Alexander Tsirulev ***

Faculty of Mathematics, Tver State University, Sadovyi per. 35, 170002 Tver, Russia; potashov.im@tversu.ru (I.P.); chemarina.yv@tversu.ru (J.T.)

* Correspondence: tsirulev.an@tversu.ru

† This article is based on the talk at the 17th International Conference on Gravitation, Cosmology and Astrophysics (RUSGRAV-17), Saint Petersburg, Russia, 28 June–4 July 2020.

Received: 16 September 2020; Accepted: 14 October 2020; Published: 16 October 2020


**Abstract:** We study geodesic motion near the throats of asymptotically flat, static, spherically symmetric traversable wormholes supported by a self-gravitating minimally coupled phantom scalar field with an arbitrary self-interaction potential. We assume that any such wormhole possesses the reflection symmetry with respect to the throat, and consider only its observable "right half". It turns out that the main features of bound orbits and photon trajectories close to the throats of such wormholes are very different from those near the horizons of black holes. We distinguish between wormholes of two types, the first and second ones, depending on whether the redshift metric function has a minimum or maximum at the throat. First, it turns out that orbits located near the centre of a wormhole of any type exhibit retrograde precession, that is, the angle of pericentre precession is negative. Second, in the case of high accretion activity, wormholes of the first type have the innermost stable circular orbit at the throat while those of the second type have the resting-state stable circular orbit in which test particles are at rest at all times. In our study, we have in mind the possibility that the strongly gravitating objects in the centres of galaxies are wormholes, which can be regarded as an alternative to black holes, and the scalar field can be regarded as a realistic model of dark matter surrounding galactic centres. In this connection, we discuss qualitatively some observational aspects of results obtained in this article.

**Keywords:** throats of wormholes; phantom scalar field; trajectories of particles; precession; gravitational lensing

**MSC:** 83C10; 83C57; 83C99

## 1. Introduction

The centres of galaxies are usually recognized to be supermassive black holes [1–3], but in fact we still do not have a completely reliable identification of these objects [4,5]. In this connection, the natural question arises as to how one may distinguish black holes from other strongly gravitating objects such as naked singularities [6,7], boson stars [8,9], and wormholes [10–13] whose properties may be very closely analogous to those of black holes [14–16]. In the context of astronomical observations, bound orbits of massive particles and trajectories of photons play a key role in dealing with this question, because they give very much information concerning the geometry of spacetime near the centres of galaxies [17–19]. However any interpretation of the observations should be based on a relevant mathematical model of geodesic motion near the central objects. In particular, dark matter surrounding the centres should be taken into account [20–23].

In this article we study the geodesic motion in the spacetime of a scalar field wormhole, connecting two asymptotically Schwarzschild universes, using a simple but completely self-consistent

approach, in which dark matter is modelled by a scalar field [24,25] while effects of rotation are not taken into account; then the problem can be analytically tractable. This approach allows us to explore some unevident features of the trajectories of massive and massless test particles in such spacetimes; these features are usually hidden in qualitative models based on computer simulations. Other useful fully analytical models are based on the Kerr-like configurations, which, however, do not take account of dark matter [4,26,27]. We will consider the simplest case of a spherically symmetric, static, traversable wormhole supported by a nonlinear self-gravitating minimally coupled phantom (in another terminology, ghost) scalar field with an arbitrary self-interaction potential. We also will assume that the wormhole connects two asymptotically flat regions of spacetime, has a single throat, and possesses the reflectional symmetry with respect to the throat. Similar models of wormholes are studied in references [28–30], and more general models are considered in references [31–34]. Distinctive features of geodesic motion near the throat of a phantom scalar field wormhole can be used to identify observationally the central objects in galaxies, and also to test general relativity in a strong gravitational regime in order to distinguish between some dark matter models and the hypothetical fifth force [35].

The paper is organized as follows. In Section 2, writing the metric of static spherially symmetric spacetime in the so-called quasiglobal coordinates, we derive and consider the main features and properties of the wormhole solutions to the Einstein-Klein-Gordon equations. Section 3 contains the mathematical description of geodesic motion in the spacetime of a static traversable scalar field wormhole which possesses the reflectional symmetry with respect to its throat. In this section, we also classify such wormholes into two qualitatively different types according to the form of the metric redshift function. We derive and analyse the behaviour of null and timelike geodesics for two analytical wormhole solutions in Section 4. Section 5 provides a brief discussion and final remarks concerning some observational aspects of geodesic motion near wormhole throats that distinguish them from other strongly gravitating objects.

The signs of the Riemann and Ricci tensor fields are defined as $R^i_{jkl} = \partial_k \Gamma^i_{jl} - \ldots$ and $R_{jl} = R^i_{jil}$, respectively. Throughout the article we adopt the metric signature $(+,-,-,-)$ and use the geometric system of units in which $G = c = 1$.

## 2. Scalar Field Wormholes

This section contains some mathematical preliminaries and relevant statements (for the most part known earlier) for studying the geodesic motion in the background of a wormhole supported by a phantom scalar field. We consider some basic properties of static spherically symmetric and asymptotically flat wormholes using the so-called inverse problem method for a self-gravitating scalar field. We begin with the action

$$S = \frac{1}{8\pi} \int \left( -\frac{1}{2} R + \varepsilon \langle d\phi, d\phi \rangle - 2V(\phi) \right) \sqrt{|g|}\, d^4x \,, \tag{1}$$

where $R$ is the scalar curvature, $V(\phi)$ is a self-interaction potential of a nonlinear scalar field $\phi$, the angle brackets denote the pointwise scalar product induced by a spacetime metric $g$, and $\varepsilon = \pm 1$. Note that $\varepsilon = -1$ corresponds to the case of a phantom scalar field. The negative sign of the kinetic term in the action (1) is a necessary condition for the existence of wormhole solutions.

For a static spherically symmetric wormhole spacetime, there exist the most natural coordinates, namely the quasiglobal coordinates, in which the metric has the form

$$ds^2 = A dt^2 - \frac{dr^2}{A} - C^2 \left( d\theta^2 + \sin^2\theta \, d\varphi^2 \right), \tag{2}$$

where the metric functions $A$ and $C$, as well as the field $\phi$, are functions only of the radial coordinate $r$ with the range from $-\infty$ to $\infty$. These functions are assumed to be of class $\mathcal{C}^2$ everywhere and to be

analytical at $r = 0$. Without loss of generality, from now on we set $r = 0$ on the throat. We restrict our attention to traversable wormholes that are symmetric with respect to the throat. This means that the metric functions are positive everywhere and invariant under the reflection:

$$A(r) > 0, \quad A(-r) = A(r), \qquad C(r) > 0, \quad C(-r) = C(r), \qquad r \in (-\infty, \infty). \tag{3}$$

The asymptotic conditions are

$$A = 1 - \frac{2M}{|r|} + O\left(|r|^{-2}\right), \quad C = |r| + \alpha + O\left(|r|^{-1}\right), \quad r \to \pm\infty, \tag{4}$$

where $M$ is the Schwarzschild gravitational mass as measured by a distant observer.

In the orthonormal basis associated with the metric (2), the independent Einstein-Klein-Gordon field equations for the action (1) are

$$-2A\frac{C''}{C} - A'\frac{C'}{C} - A\frac{C'^2}{C^2} + \frac{1}{C^2} = \varepsilon A\phi'^2 + 2V\,, \tag{5}$$

$$A'\frac{C'}{C} + A\frac{C'^2}{C^2} - \frac{1}{C^2} = \varepsilon A\phi'^2 - 2V\,, \tag{6}$$

$$-A\phi'' - \phi'\left(A' + 2A\frac{C'}{C}\right) + \varepsilon\frac{dV}{d\phi} = 0\,, \tag{7}$$

where a prime denotes differentiation with respect to the radial coordinate $r$. Both for classical and phantom scalar fields, there exists a special algorithm, the so-called 'inverse problem method for self-gravitating scalar field', for constructing one-parameter families of static spherically symmetric solutions to the Einstein-Klein-Gordon equations. This method developed in references [36–40] allows us to examine the problem, in some sense, for all admissible self-interaction potentials at the same time. We will use a variant of the inverse problem method in which a 'general' solution of Equations (5)–(7) is represented by simple quadratures [41].

In the case under consideration (namely, $\phi$ is a phantom field with $\varepsilon = -1$, and the conditions (3) and (4) hold), the quadratures have the form

$$A = 2C^2\int_r^\infty \frac{r}{C^4}\,dr, \tag{8}$$

$$\phi'^2 = C''/C, \tag{9}$$

$$\widetilde{V}(r) = \left(1 - 3AC'^2 - ACC'' + 2rC'/C\right)/\left(2C^2\right), \tag{10}$$

$$V(\phi) = \widetilde{V}\left(r(\phi)\right). \tag{11}$$

It is not hard to verify that expressions (8)–(10) reduce Equations (5)–(7) to identities. Moreover, one can formulate the converse as follows: if $(A, C, \phi)$ is a solution of Equations (5)–(7) for a given potential $V$, and if the conditions (3) and (4) hold, then the relations (8)–(11) are true. From Equation (9), which is the sum of (5) and (6) divided by $-2A$, one sees that $C''(r) \geq 0$ everywhere. It means that if $C''(0) \neq 0$, then $\phi(r)$ is necessarily an odd function. If $C''(0) = 0$, then the field can be thought of either as an even or odd function. In order to avoid multiple repetitions and for definiteness, we will consider analytically only the right half of a wormhole (that is, the region $r \geq 0$) and extend $\phi(r)$ to the left half as an odd function.

A convenient mathematical technique for constructing wormhole solutions consists of the following steps: first, one should specify an appropriate function $C(r)$; second, it is necessary to calculate the metric function $A(r)$, the field $\phi(r)$, and the potential $\widetilde{V}(r)$ as a function of the radial coordinate; finally, taking into account that $\widetilde{V}(r)$ is necessarily an even function, the self-interaction potential $V(\phi)$ can be restored by the formula (11). Another way of constructing the solutions is

to specify a monotonic field function $\phi(r)$, and then to solve the equation $C'' - \phi'^2 C = 0$ for $C(r)$. Note also that the condition (4) and the quadrature (8) allow us to write the metric (2) at infinity in the Schwarzschild coordinates; we find that the Schwarzschild mass is uniquely determined by the constant $\alpha$, and is given by

$$M = \alpha/3. \tag{12}$$

We will suppose below that $M > 0$ because the gravitational field of a zero mass wormhole does not approach to the Newtonian limit at infinity. For example, if $C = r + p/r + q/r^2 + o(r^{-2})$ $(q \neq 0)$ as $r \to +\infty$, then one find from (8) that $A = 1 + 2q/(5r^3) + O(r^{-4})$. It shows that such a wormhole possesses a non-Newtonian gravitational potential $\left(\text{namely, } \Phi = q/(5r^3)\right)$. Moreover, if $q > 0$, the gravitational force is repulsive.

As a consequence of the condition (3), the expansions of the metric functions in the vicinity of the throat have the form

$$A = A_0 + \frac{1}{2}A''(0)r^2 + \frac{1}{24}A^{(4)}(0)r^4 + \ldots, \qquad C = C_0 + \frac{1}{2}C''(0)r^2 + \frac{1}{24}C^{(4)}(0)r^4 + \ldots. \tag{13}$$

Directly from (8) and (13) we find that

$$A_0 = 2C_0^2\int_0^\infty \frac{r}{C^4}\,dr, \quad A''(0) = \frac{2}{C_0^2}\left(A_0C_0C''(0) - 1\right), \quad A^{(4)}(0) = \frac{2A_0}{C_0^2}\left(C_0C^{(4)} + 3[C''(0)]^2\right). \tag{14}$$

It follows from (4), (8), and (12) that $A' = 2Mr^{-2} + O(r^{-3})$ as $r \to +\infty$, that is, $A' > 0$ in some neighbourhood of the (positive) spatial infinity, and therefore $A(r)$ reaches its minimum value at some point $r = r_{min} \geq 0$ in a coordinate neighbourhood of the throat; in the case $r_{min} > 0$, we will assume that $A(r)$ decreases in the region $(0, r_{min})$. These arguments imply that there are two geometrically and observationally different types of wormhole configurations. In wormhole spacetimes of the first type (respectively, second type), the metric function $A(r)$ reaches a minimum (respectively, maximum) at the throat. The minimum (respectively, maximum) at $r = 0$ takes place if and only if there exists an integer $n \geq 1$ such that

$$A^{(2k)}(0) = 0 \ \ (k = 1, \ldots, n-1), \qquad A^{(2n)}(0) > 0 \ \ (\text{respectively, } A^{(2n)}(0) < 0). \tag{15}$$

Note that we exclude from our consideration the special case $A \equiv 1$ represented by the unique (apart from flat spacetime) Ellis–Bronnikov solution [42–45] with $\phi(r) = \arctan(r/C_0)$, $V(\phi) = 0$, and $C(r) = \left(r^2 + C_0^2\right)^{1/2}$; this solution represents a traversable wormhole which is geodesically complete but admits no stable bound orbits at all.

In what follows, we take, for the sake of brevity, $n = 1$ in (15). This restriction is motivated by numerical experiments which have shown that the qualitative behaviour of geodesics for $n = 1$ is essentially the same as for $n \geq 2$. Then it follows directly from (14) that the conditions (15) can be rewritten in the form

$$A_0C_0C''(0) - 1 > 0 \ \ (\text{for the first type}), \quad A_0C_0C''(0) - 1 < 0 \ \ (\text{for the second type}). \tag{16}$$

In particular, a wormhole is of the second type if $C''(0) = 0$. Note that the constant $C_0$ is the size of the throat, and $A_0$ can be interpreted either as the potential barrier height (if $A''(0) < 0$) or as the potential well depth (if $A''(0) > 0$) for test particles falling radially toward the throat.

The geometrical system of units does not fix a unit of length. On the other hand, the geodesic structure of spacetime is scale invariant at the classical level, and Equations (5)–(7) and the quadratures (8)–(11) are also invariant under the scale transformations

$$r \to r/\lambda, \quad M \to M/\lambda, \quad V \to \lambda^2 V, \qquad \lambda > 0.$$

Therefore, we can use an arbitrary unit of length. By applying $\lambda = M$ in this transformation, we can take, as it is usually done in general relativity, the Schwarzschild mass of a configuration as the current unit of length. Thus, without loss of generality, we suppose everywhere below that $M = 1$.

## 3. Timelike and Null Geodesics

In all stationary spherically symmetric spacetimes we have the conserved energy and angular momentum of a test particle. Together with the constancy of the norm of the four-velocity, this implies the existence of three integrals of motion [46]. Supposing that a particle moves in the equatorial plane, these integrals for the metric (2) can be written in the form

$$C^2\frac{d\varphi}{ds} = J\,, \quad A\frac{dt}{ds} = E\,, \quad \left(\frac{dr}{ds}\right)^2 = E^2 - V_{eff}, \tag{17}$$

$$V_{eff} = A\left(\mathrm{k} + \frac{J^2}{C^2}\right), \tag{18}$$

where $J$ is the specific angular momentum, and $E$ is the specific energy of a test particle. For massive test particles, $\mathrm{k} = 1$ and $s$ is the proper time, while for massless ones $\mathrm{k} = 0$ and $s$ is an arbitrary affine parameter. The effective potential $V_{eff}$ is obviously an even function, and $V_{eff} \to 1$ ($V_{eff} \to 0$) for massive particles (respectively, for massless ones) as $r \to \infty$.

From the point of view of a distant observer at rest with respect to the centre, the angular velocity of a test particle along its trajectory is given by

$$\omega = \frac{d\varphi}{dt} = \frac{J}{E}\frac{A}{C^2}$$

both for null and timelike geodesics. Note that $\omega = 0$ for massive particles in the resting-state stable circular orbit where $J = 0$.

### *3.1. Timelike Geodesics*

Let $C$ be specified and $A$ be found from (8). Then any timelike geodesic is determined by its arbitrary point and the parameters $J$ and $E$. We are primarily interested in circular orbits of massive particles near the throats of wormholes, so that we set $\mathrm{k} = 1$ in this section. From (18) we have

$$V'_{eff}(r, J) = A' + J^2\left(\frac{A}{C^2}\right)', \tag{19}$$

where a prime denotes differentiation with respect to $r$. Circular orbits correspond to solutions of the equation $V'_{eff}(r, J) = 0$. For circular orbits in the region $r > 0$, the $r$-component of the geodesic equation gives

$$A'\left(\frac{dt}{ds}\right)^2 - \left(C^2\right)'\left(\frac{d\varphi}{ds}\right)^2 = 0. \tag{20}$$

This relation together with (17) allows us to express the first two integrals of (circular) motion as functions only of the radial coordinate:

$$J^2 = C^2\frac{A'}{A}\left(2\frac{C'}{C} - \frac{A'}{A}\right)^{-1}, \quad E^2 = 2A\frac{C'}{C}\left(2\frac{C'}{C} - \frac{A'}{A}\right)^{-1}.$$

On the right side of a wormhole, timelike circular orbits may exist only in the region where the conditions $A' > 0$ and $2C'/C - A'/A > 0$ hold; the latter is equivalent to

$$\left(A/C^2\right)' < 0. \tag{21}$$

It follows directly from (8) that $\left(A/C^2\right)' < 0$ for all $r > 0$. In wormholes of the first type, the condition $A' > 0$ holds for all $r > 0$. However, in wormholes of the second type, this condition holds only in the region $r > r_{min}$. On the throat, the limit equality $\left(A/C^2\right)' = 0$ is identically satisfied due to the conditions (13).

Massive particles, moving along circular orbits close to the throat, may or may not form an accretion disk, which in turn may or may not have the innermost stable circular orbit. Let us first consider wormholes of the first type for which $A''(0) > 0$, $A'(0) = C'(0) = 0$; the latter implies $V'_{eff} = 0$. Taking into account the second equality in (14), we find from (18) that

$$V''_{eff}(0, J) = A''(0) - \frac{2J^2}{C_0^4}, \qquad V''_{eff}(0, J) = 0 \;\Rightarrow\; J = J_0 \equiv C_0^2 \frac{\sqrt{A''(0)}}{2}. \tag{22}$$

The value $J_0 = C_0^2\sqrt{A''(0)/2}$ separates stable and unstable orbits located at the throat. Such an orbit is stable if $J < J_0$, and, moreover, particles in orbits with $J = 0$ are at rest. If $J > J_0$, then orbits located at $r = 0$ are unstable, but for each $r > 0$ there exists a stable orbit. Indeed, if $V''_{eff}(0) < 0$ and $V'_{eff} > 0$ at infinity, the effective potential has a minimum at some point $r = r_* > 0$ at which $V''_{eff} > 0$. On the other hand, it follows from (19) and (21) that there exists a unique solution, say $r_*(J)$, of the equation $V'_{eff}(r, J) = 0$ for each $J > J_0$. Moreover, we have the inequality

$$V'_{eff}(r_*, J) = 0 \quad \Rightarrow \quad \frac{dr_*}{dJ} = -\frac{1}{V''_{eff}}\frac{dV'_{eff}}{dJ}\Big|_{r=r_*} = -\frac{2J}{V''_{eff}}\left(\frac{A}{C^2}\right)'\Big|_{r=r_*} > 0, \tag{23}$$

which shows that the coordinate radius $r_*$ of the stable circular orbit increases monotonically as $J$ increases. For circular orbits close to the throat this fact is not self-evident, because in this region the spacetime geometry of wormholes is radically different from the geometry of black holes.

These arguments remain in force for wormholes of the second type, but in this case stable circular orbits exist only in the region $r \geq r_{min} > 0$, and particles are at rest ($J = 0$) in the orbit with $r = r_{min}$, where $r_{min}$ is defined after the expressions (14). Thus, an important result of our analysis is that a scalar field wormhole can have a continuous accretion disk which stretches from some $r = r_{min} \geq 0$ to the orbit of a source of diffuse matter revolving around the wormhole. For definiteness, we will refer to any orbit at $r = r_{min} > 0$ as the resting-state stable circular orbit: its difference from the innermost stable circular orbit ($r_{min} = 0$) is that particles in the resting-state stable circular orbits are at rest with respect to the throat or have an observationally negligible velocity. The radius of the resting-state stable circular orbit equals $C_0$ for a wormhole of the first type, while for that of the second type it can be much greater than $C_0$.

Other important astrometric characteristics of bound orbits in the central regions are deviations from the vacuum (Schwarzschild) orbital form. Nowadays the most simple and informative observational data are provided by the precession of pericentres of stellar orbits located close to the centres. We can express the angle of precession $\Delta\varphi$ of a bound orbit directly from (17) as

$$\Delta\varphi = \varphi_{osc} - 2\pi, \qquad \varphi_{osc} = 2J\int_{r_p}^{r_a} \frac{dr}{C^2\sqrt{E^2 - V_{eff}}}, \tag{24}$$

where $r_p$ and $r_a$ are the pericentre and apocentre radii, respectively. In other words, they are solutions of the equation $E^2 - V_{eff} = 0$ such that $r_p < r_J < r_a$, where $r_J$ is a (global or local) minimum of $V_{eff}(r, J)$, and there are no other solutions in the interval $(r_p, r_a)$. Thus, a bound orbit of the general type oscillates near a stable circular orbit (an oscillation is the motion from pericentre to apocentre and back) and $\varphi_{osc}$ is the polar angle which has been passed around the centre between any two successive pericentre points of the orbit. The relativistic precession of pericentres of bound orbits is considered

in [9,22,35,47–50] both from a purely theoretical point of view and in the context of observations of S-stars in the Galactic Centre.

### *3.2. Null Geodesics*

For null geodesics k = 0, so that (17) and (18) can be rewritten in the form

$$C^2\frac{d\varphi}{d\lambda} = b\,, \quad A\frac{dt}{d\lambda} = 1\,, \quad \left(\frac{dr}{d\lambda}\right)^2 = 1 - b^2\frac{A}{C^2}, \tag{25}$$

where $\lambda = sE$ is a new affine parameter, and $b = J/E$ is the impact parameter. Thus, the behaviour of a null geodesic is determined only by its arbitrary point and the unique, as opposed to a timelike geodesic, parameter $b$. We will not consider the trivial case $b = 0$ corresponding to a radially falling photon. The spatial trajectory of a photon satisfies the differential equation

$$\frac{dr}{d\varphi} = \pm C^2\sqrt{\frac{1}{b^2} - \frac{A}{C^2}}. \tag{26}$$

An obvious necessary condition for the existence of a null geodesic with a given $b$ is

$$\frac{1}{b^2} \geq \frac{A}{C^2},$$

where the equality holds only at the turning point (the point of closest approach to the throat) or in an unstable circular orbit at the throat. Another important condition for null geodesics also follows directly from (25): the trajectory of a photon crosses the throat if and only if

$$\frac{1}{b^2} \geq \frac{A_0}{C_0^2} = 2\int_0^\infty \frac{r}{C^4}\,dr. \tag{27}$$

If this condition holds, then the photon leaves forever, in contrast to bound timelike geodesics, the region $r < 0$.

## 4. Two Examples of Wormholes

In this section we explore two examples of static wormhole solutions that have not been considered in the literature earlier. They are based on the ansatz

$$C = \left(r^4 + 2r^2 + a^2\right)^{1/4} + 3, \quad a \geq 1, \tag{28}$$

where $a$ is the parameter of 'intensity' of the scalar field. In accordance with the conditions (4), (12), and the remark at the end of Section 2, all wormholes in the family (28) are of unit mass, $M = 1$. For simplicity we will consider wormholes with $a = 1$ and $a = 9$. For these values of $a$, the metric function $A(r)$ can be obtained in terms of elementary functions and elliptic functions, respectively, but we have not written the explicit expressions for $A(r)$ because of their cumbersome forms. The self-interaction potential $\widetilde{V}(r)$ is partially negative (in the region $(p, \infty)$, $p > 0$) for all $a \geq 1$, and the field $\phi(r)$ is an odd function. The effective potentials $V_{eff}(r, J)$ of timelike geodesics and the function $A(r)$ are shown in Figure 1. Below in this section we will need an explicit expression for the unique solution $J_*$ of the equation $V_{eff}(0, J) = 1$; from (18) we find

$$J_* = C_0\sqrt{1/A_0 - 1}\,. \tag{29}$$

It should be stressed that bound orbits can exist only in the region where $A < 1$. Note also that we consider examples whose types can be clearly recognized: for $a = 1$ and $a = 9$, the wormholes

are of the first and second types, respectively. The effective potentials $V_b(r,b) = 1 - b\left(A/C^2\right)$ of null geodesics are shown in Figure 2.

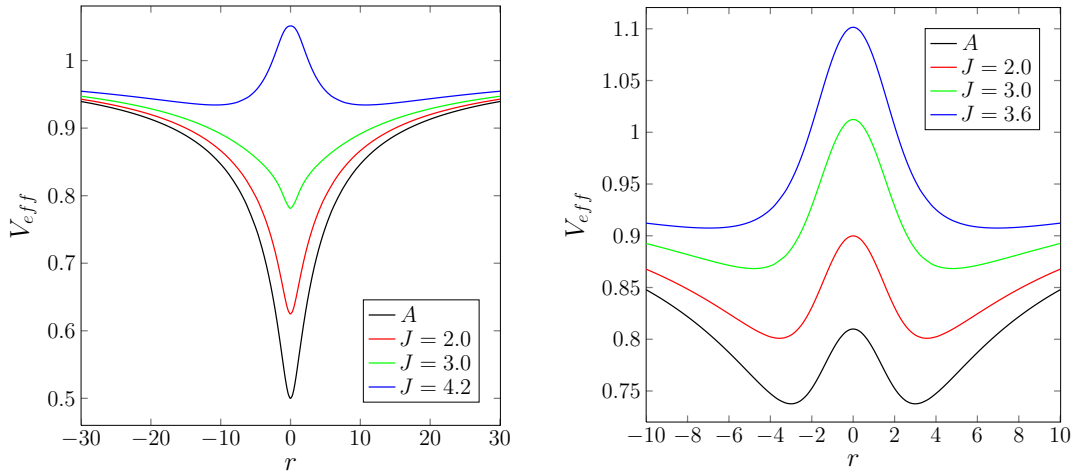


**Figure 1.** The effective potentials $V_{eff}(r,J)$ of massive particles and (if $J = 0$) the metric function $A(r) = V_{eff}(r,0)$ for the ansatz (28): $a = 1$ (**left panel**) and $a = 9$ (**right panel**).

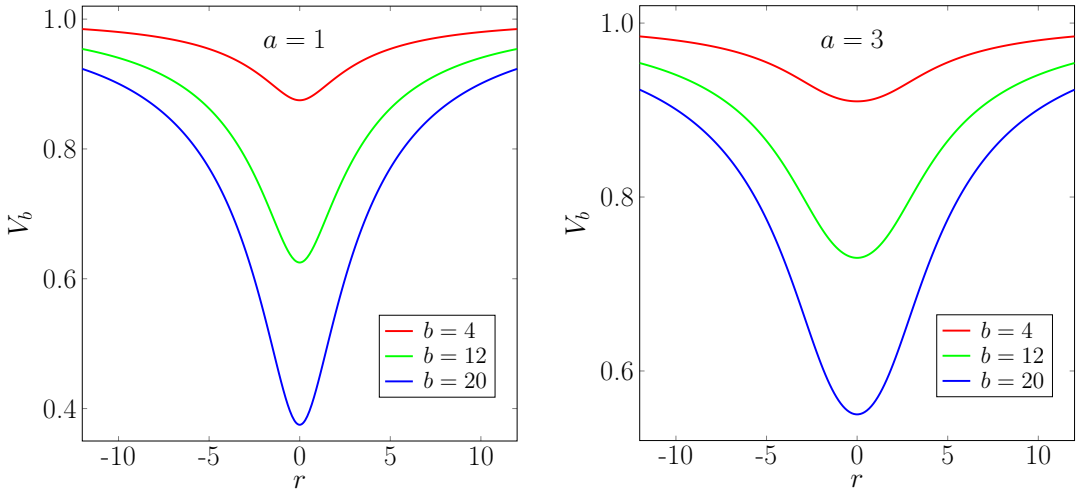


**Figure 2.** The effective potentials $V_b(r,b) = 1 - b\left(A/C^2\right)$ of massless particles for the ansatz (28): $a = 1$ (**left panel**) and $a = 9$ (**right panel**).

### *4.1. Trajectories of Timelike Geodesics*

In our analysis of bound orbits around the throat, we are interested in two the most important observational parameters: the angle of pericentre precession and the radius of the innermost (or resting-state) stable circular orbit of the accretion disk. Both the characteristics crucially depend on the type of wormhole.

The possible shapes of orbits are represented in Figures 3 and 4. Note that in this, and in the next subsections, we represent all the orbit trajectories in the polar Schwarzschild-like coordinates, that is, as functions $C(\varphi)$ but not $r(\varphi)$. We see that there exist two distinct kinds of orbits: orbits of the first kind (second kind) are shown in the left panels (respectively, right panels) of these figures. Orbits of the first kind cross the wormhole throat, so that the parts of their trajectories that are located in the region $r < 0$, and shown by dashed lines in the figures, should be considered as hidden behind the throat. Therefore, for such orbits, the angle of precession, $\Delta\varphi$, of an orbit should be determined observationally as the angular size of the observed trajectory of the orbit (that is, the angle between an entry point in the region $r > 0$ and the next exit point) minus $2\pi$; in other words, it should be

set $r_p = 0$ for the lower limit of integration in (24). It is obvious from the equality (22) and is shown in the left panel of Figure 1 that any wormhole of the first type has its own value $J_0$ of the specific angular moment such that orbits, independently of the specific energy $E$, are of the first kind if $J < J_0$; for $J > J_0$, an orbit is of the first kind and of the second kind if, respectively, $V_{eff}(0, J) \leq E^2 < 1$ and $V_{eff}(r_*(J), J) < E^2 < V_{eff}(0, J)$, where $r_*(J)$ is determined by Equation (23); orbits with $E \geq 1$ are not bound, since $V_{eff} \to 1$ as $r \to \infty$.

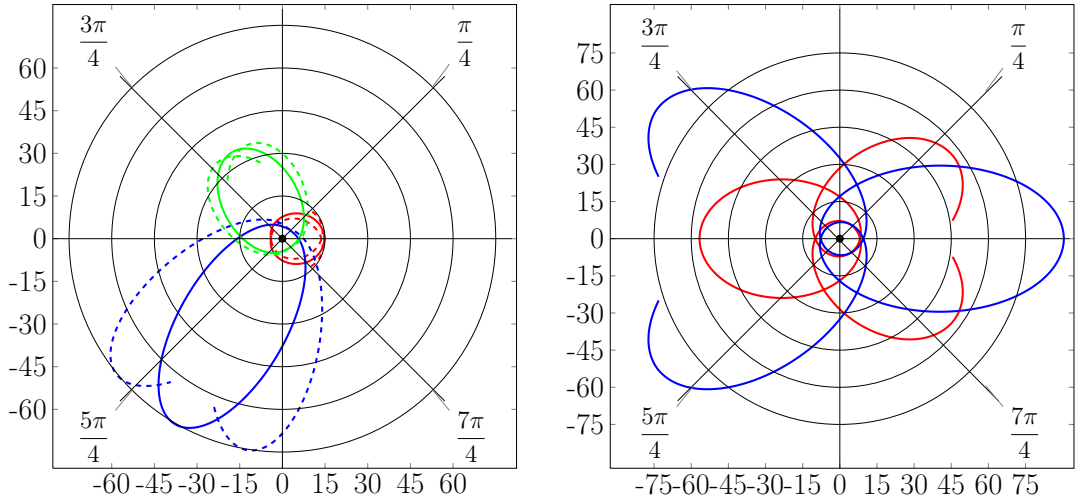


**Figure 3.** The shapes of some precessing trajectories of massive test particles for ansatz (28) with $a = 1$. **Left panel** ($J = 3$): $E^2 = 0.90$, $\Delta\varphi = 0.31$ (red line), $E^2 = 0.95$, $\Delta\varphi = -0.18$ (green line), $E^2 = 0.975$, $\Delta\varphi = -0.36$ (blue line). The dashed parts of lines represent the 'hidden' parts of trajectories located in the region $r < 0$. **Right panel** ($J = 4.2$): $E^2 = 0.97$, $\Delta\varphi = 2.52$ (red line), $E^2 = 0.98$, $\Delta\varphi = 2.70$ (blue line).

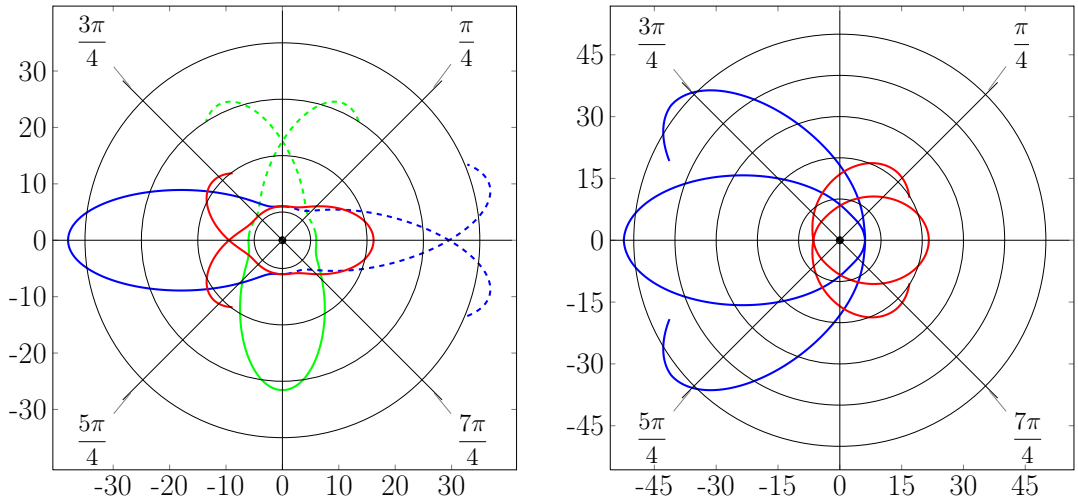


**Figure 4.** The shapes of some precessing trajectories of massive test particles for ansatz (28) with $a = 9$. **Left panel** ($J = 2$): $E^2 = 0.89$, $\Delta\varphi = -2.44$ (red line), $E^2 = 0.93$, $\Delta\varphi = -2.76$ (green line), $E^2 = 0.95$, $\Delta\varphi = -2.89$ (blue line). The dashed parts of lines represent the parts of trajectories located in the region $r < 0$. **Right panel** ($J = 3$): $E^2 = 0.925$, $\Delta\varphi = -0.82$ (red line), $E^2 = 0.965$, $\Delta\varphi = -0.64$ (blue line).

In a wormhole of the second type, the classification of bound orbits, as can be seen directly from Figure 1 (right panel), depends on whether $0 < J < J_*$ or $J > J_*$, where $J_*$ is determined by the expression (29). Let the first condition be true. Then an orbit is of the first kind if $V_{eff}(0, J) \leq E^2 < 1$; an orbit is of the second kind if $V_{eff}(r_*(J), J) \leq E^2 < V_{eff}(0, J)$. If $J > J_*$ and $V_{eff}(r_*(J), J) \leq E^2 < 1$, then an orbit is always of the second kind. In other cases bound orbits in a wormhole of the second

type do not exist. Note that $J_0$, $J_*$, and $r_{min}$ are determined only by a given wormhole spacetime (in our case, by the function $C(r)$), while $r_*$ depends on $J$. However, this fact is not important in our analysis because there are no orbits with $E^2 < V_{eff}(r_*(J), J)$.

For both the types of wormholes under consideration, the angle of precession of orbits of the first kind decreases and attains negative values with increasing the specific energy $E$ when the value of $J$ is fixed. Orbits of the second kind are completely located in the 'right' halves of wormholes. The angle of precession of such an orbit, in contrast to orbits of the first kind, increases with increasing the specific energy $E$ and at a fixed $J$. It also turns out that for orbits of the second kind, $\Delta\varphi$ is always positive in wormholes of the first type; but in wormholes of the second type, $\Delta\varphi < 0$ for orbits that pass sufficiently close to the throat. The various numerical experiments with wormhole solutions allow us to conclude that these properties hold generally and therefore can be used in astronomical observations in order to distinguish scalar field wormholes from scalar field naked singularities [49] and scalar field black holes [50].

It can be seen directly from the left panel in Figure 1 that wormholes of the first type can have a continuous accretion disk with the observable innermost stable circular orbit whose radius equals the radius of the throat $C_0 = C(0)$. In the first example ($a = 1$) we have $C_0 = 4$, $0 \leq J \lesssim 3.82$, and $4.97 \lesssim E^2 \lesssim 9.61$. In the innermost stable circular orbit, particles are expected to have a maximum possible specific angular momentum, because any such particle has spiraled into this orbit from an outer orbit as a result of the loss of its energy and angular momentum: in the first example, $J_{ISCO} \approx 3.82$ and $E^2_{ISCO} \approx 9.61$. It can also be expected that the throat (in this context, the visible inner edge of the accretion disk) appears to be bright enough, since the motion of particles in the neighbourhood of the throat should be slightly chaotic, but enough to form a turbulent flow.

In contrast, a wormhole of the second type can be characterized by the condition $r_{min} = r_*(0)$, where $r_*(0)$ is the unique solution of the equation $V'_{eff}(r, 0) = 0$ (or, equivalently, $A'(r) = 0$). Therefore, the wormhole does not have the innermost stable circular orbit, but instead has the resting-state stable circular orbit whose radius, $C(r_{min})$, always greater than $C_0$ (see last but one paragraph in Section 3.1). In a sufficiently small neighborhood of the sphere of radius $r_{min}$, a particle can be at rest at all times in the resting-state stable circular orbit or can slowly move near it in an orbit of small eccentricity. Therefore, the wormhole will have a classical-like accretion disk if the baryonic matter surrounding the wormhole had been accreting onto it for a sufficiently short period of cosmic time before observations. In this case, the luminosity of the disk in the vicinity of its inner edge increases with increasing $r$. The particles will spread out with time from the inner edge into a thin spherical shell of radius $r_{min}$. Thus, for an 'old' wormhole with high accretion activity in the outer region, one can expect to see such a shell together with the adjoining inner edge of the accretion disk; both will be of small but nonzero brightness and will consist of 'grey' dust, gas, or fluid.

### *4.2. Trajectories of Null Geodesics*

Similarly to the case of massive test particles, there exist two kinds of null geodesics in a wormhole spacetime: a geodesic of the first kind passes through the wormhole throat, while a geodesic of the second kind remains in the region $r \geq 0$. A null geodesic is of the first kind if and only if the condition (27) holds. Geodesics of the first kind (second kind) are shown in the left panel (respectively, right panel) of Figures 5 and 6.

We will assume that the apparent luminosity of sources, placed at large distance from the wormhole, is very small. Then the image of a wormhole, that is, the shape and brightness of the wormhole accretion disk, is determined by the behaviour of null geodesics of both these kinds, together with the inclination of the disk plane with respect to the line of sight of an observer. In general, an analytical computation of this image for scalar field wormholes seems to be impossible, therefore we will briefly discuss these issues qualitatively in the same standard manner as for black holes [4,7,14,17,26,27].

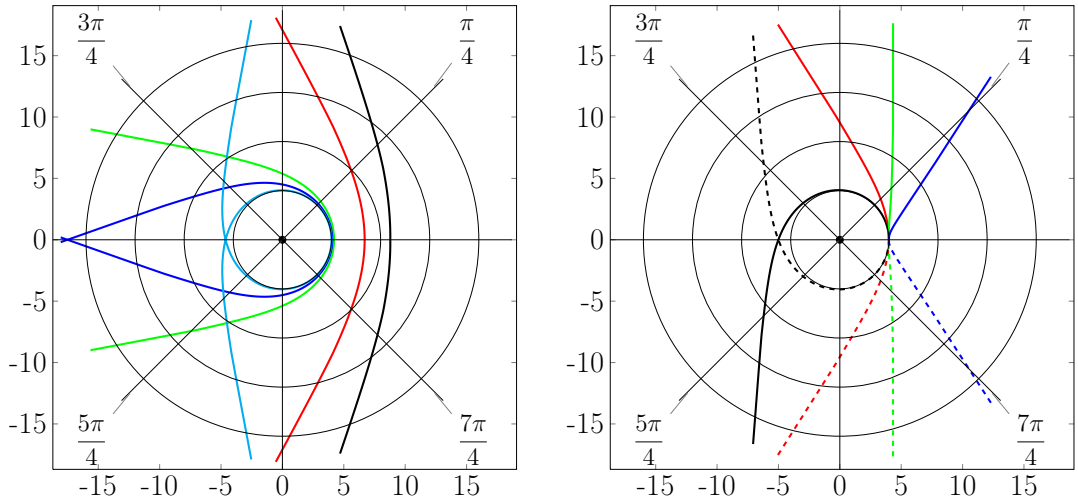


**Figure 5.** Photon trajectories of massive test particles for ansatz (28) with $a = 1$. In the **left** plot: $b = 10$ (black line), $b = 8$ (red line), $b = 5.8$ (green line), $b = 5.7$ (blue line), $b = 5.66$ (cyan line). In the **right** plot: $b = 5.65$ (black line), $b = 5$ (red line), $b = 4.2$ (green line), $b = 3$ (blue line). The dashed parts of lines represent the parts of trajectories located in the region $r < 0$.

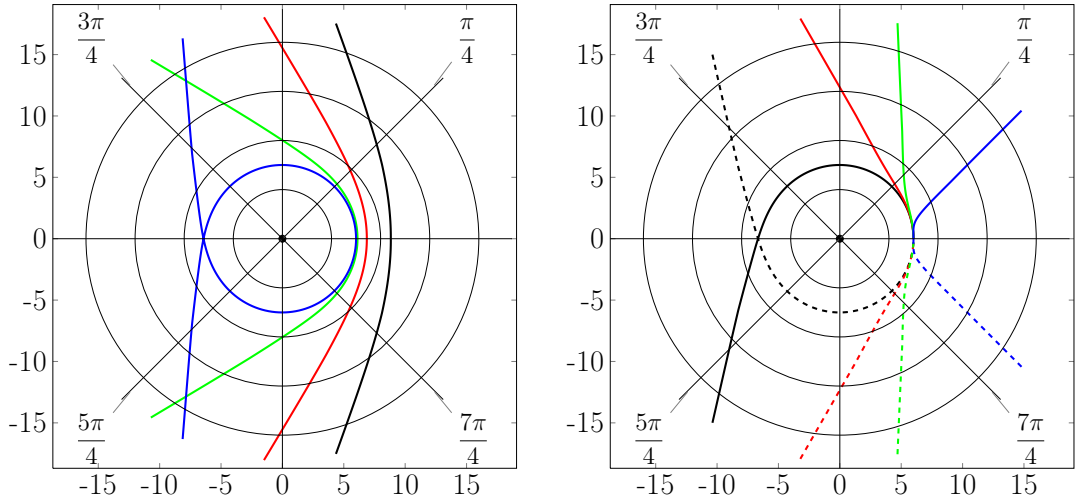


**Figure 6.** Photon trajectories of massive test particles for ansatz (28) with $a = 9$. In the **left** plot: $b = 10$ (black line), $b = 8$ (red line), $b7$ (green line), $b = 6.7$ (blue line). In the **right** plot: $b = 6.65$ (black line), $b = 6$ (red line), $b = 5.3$ (green line), $b = 3$ (blue line). The dashed parts of lines represent the parts of trajectories located in the region $r < 0$.

If a wormhole of the first type with high accretion activity has the inner edge of the accretion disk to be placed at the throat, then an observer will see also the dual part of the disk placed in the region $r < 0$. This means that the observer will see a continuous disk without a central dark spot; it can be seen directly from Figure 5 (right panel). As it is shown above, a wormhole of the second type with high accretion activity has a grey spherical shell of the observed radius $C(r_{min})$. Thus, in fact, the wormholes of interest are those that exhibit a low accretion activity and have a sufficiently large radius of the visible inner edge of the accretion disk. In this case, the vicinity of the disk near the visible inner edge should be bright (should be grey) in wormholes of the first type (respectively, of the second type). This situation is illustrated in the left panels of Figures 5 and 6 for both the first and second types of wormholes.

One way to represent trajectories of photons coming from the left half of a wormhole (and, consequently, the image of bright matter located in the left half) consists in the following.

A static wormhole has the topology $\mathbb{R} \times \sum$, where $\mathbb{R}$ is 'time', and the 'space' $\sum$ is the connected sum of two copies of $\mathbb{R}^3 \backslash \mathbb{B}^3_{C_0}$; the boundary of the ball $\mathbb{B}^3_{C_0}$ is obviously the throat of the wormhole. It is convenient to immerse the wormhole into $\mathbb{R}^3$ with spherical coordinates $(\tilde{r}, \theta, \varphi)$: one cuts out the central ball $\mathbb{B}^3_{C_0}$ from $\mathbb{R}^3$ and defines the immersion (it looks like a Riemann surface) explicitly by the map $(\pm r, \theta, \varphi) \mapsto (\tilde{r} - C_0, \theta, \varphi)$. If a photon passes through the throat, then its trajectory in $\mathbb{R}^3 \backslash \mathbb{B}^3_{C_0}$ consists of two parts which are located in the same plane and possess the reflection symmetry with respect to the perpendicular to the throat in the intersection point.

Let us assume for simplicity that the line of sight of an observer is perpendicular to the disk plane. Then, it can be expected that a distant observer will see, first, the outer accretion disk with the inner radius $C(r_*(J))$ (the first type, $J > J_0$) or $C(r_{min})$ (the second type). Second, he will see a bright ring of the radius $C_0$ made up of photons in unstable circular orbits at the throat (the photon sphere). It is also possible that the observer will also see the inner accretion disk (of the outer radius $C_m < C_0$), that is, the image of the dual part (placed in the region $r < 0$) of the total accretion disk. In any case, this picture is radically different from that for black holes.

## 5. Discussion

In this article, we have examined two types of scalar field wormholes and found some distinctive features of timelike bound orbits located in the vicinities of the wormhole throats, and of the trajectories of null geodesics. In our approach, a scalar field models dark matter surrounding the centres of normal galaxies. The most important aspect of our results is that they can help to distinguish between wormholes and other possible types of strongly gravitating objects in galaxies using astronomical observations of orbital precessions, accretion disks, and the 'images' of the central dark (or grey) regions. Here, for definiteness, we compare wormholes with Schwarzschild black holes.

We have seen that orbits that are sufficiently close to the centre of a wormhole exhibit considerable retrograde precession (the angle of pericentre precession is negative), while those that for the most part are in the region of Schwarzschild gravity have small negative or positive precession angles: this can be seen from the comparison of the left and right panels in Figures 3 and 4. Moreover, the effect of retrograde precession is more significant for wormholes of the second type, and, also, the angle of pericentre precession increases with increasing the specific angular momentum $J$. However, the modern astrometric accuracy is not enough to observe these effects confidently. For example, the orbits in right panels of Figures 3 and 4 have the pericentre distance of order of the size of the throat, namely $\approx$5 and $\approx$7 (in geometrical units with $M = 1$), respectively. Note that Schwarzschild black holes always exhibit only the prograde relativistic precession of pericentres. On the other hand, the angle of pericentre precession for S-stars in the centre of our Galaxy can be measured today in the region $C \gtrsim 2000$ ($\sim$100 AU for $M \sim 4 \cdot 10^6\, M_\odot$). In order to detect a meaningful deviation from the Schwarzschild precession, the accuracy of the measurements should be at least an order of magnitude larger than what has been achieved now.

Observations of the accretion disk of a wormhole seems to be more consistent with the present-day astronomical instrumentation, and therefore to be more informative to compare with the observations of star orbits. In this connection, it is necessary to mention the following three important points. First, it is well-known that the spot in the centre of image of a Schwarzschild black hole, known as the black hole shadow, has the observed radius $C_{sh} \approx 5.2$ in geometrical units with $M = 1$. On the other hand, the visible inner edge of the accretion disk in a wormhole spacetime can have an arbitrary value of the observed radius $C_d$ in the range $C_d \geq C_0$ or $C_d \geq C(r_{min})$ according to whether the wormhole is of the first or second type, respectively; thus, $C_d$ does not depend directly on the wormhole mass. Second, assuming that the background radiation of the sky is negligible in comparison with that of the accretion disk, this central spot should be dark. In contrast, in wormholes of the second type with high accretion activity, the grey shell, surrounding the throat, is expected to be of small but nonzero brightness. Third, a black hole is expected to have a bright ring of the observed radius $C_{ph} = 3$ formed by photons moving in spiral orbits from the photon sphere to infinity. Wormholes of the second type

with small accretion activity also can have such a photon ring, but the brightness of the accretion disk in the vicinity of its inner edge should be very small.

**Author Contributions:** Conceptualization, A.T.; investigation, I.P., J.T., and A.T.; software, I.P.; visualization, I.P. and J.T.; writing—original draft preparation, J.T. and A.T.; and writing—review and editing, A.T. The order of authors is alphabetical. All authors have read and agreed to the published version of the manuscript.

**Funding:** This research received no external funding.

**Acknowledgments:** The authors are grateful to the reviewers for their valuable remarks and comments.

**Conflicts of Interest:** The authors declare no conflict of interest.

## References

1. Goddi, C.; Falcke, H.; Kramer, M.; Rezzolla, L.; Brinkerink, C.; Bronzwaer, T.; Eatough, R.P. BlackHoleCam: Fundamental physics of the Galactic center. *Int. J. Mod. Phys. D* **2017**, *26*, 1730001. [CrossRef]
2. Akiyama, K. et al. [The EHT Collaboration] First M87 Event Horizon Telescope Results. I. The Shadow of the Supermassive Black Hole. *Astrophys. J. Lett.* **2019**, *875*, L1.
3. Abuter, R. et al. [GRAVITY Collaboration] Detection of the Schwarzschild precession in the orbit of the star S2 near the Galactic centre massive black hole. *Astron. Astrophys.* **2020**, *636*, L5.
4. Johannsen, T. Sgr A* and general relativity. *Class. Quant. Grav.* **2016**, *33*, 113001. [CrossRef]
5. Perlick, V.; Tsupko, O.Y.; Bisnovatyi-Kogan, G.S. Influence of a plasma on the shadow of a spherically symmetric black hole. *Phys. Rev. D* **2015**, *92*, 104031. [CrossRef]
6. Joshi, P.S.; Malafarina, D.; Narayan, R. Distinguishing black holes from naked singularities through their accretion disc properties. *Class. Quant. Grav.* **2014**, *31*, 015002. [CrossRef]
7. Shaikh, R.; Kocherlakota, P.; Narayan, R.; Joshi, P.S. Shadows of spherically symmetric black holes and naked singularities. *Mon. Not. R. Astron. Soc.* **2018**, *482*, 52–64. [CrossRef]
8. Macedo, C.F.B.; Pani, P.; Cardoso, V.; Crispino, L.C.B. Astrophysical signatures of boson stars: Quasinormal modes and inspiral resonances. *Phys. Rev. D* **2013**, *88*, 064046. [CrossRef]
9. Grould, M.; Meliani, Z.; Vincent, F.H.; Grandclément, P.; Gourgoulhon, E. Comparing timelike geodesics around a Kerr black hole and a boson star. *Class. Quant. Grav.* **2017**, *34*, 215007. [CrossRef]
10. Bronnikov, K.A.; Fabris, J.C. Regular fantom black holes. *Phys. Rev. Lett.* **2006**, *96*, 251101. [CrossRef]
11. Bronnikov, K.A.; Dehnen, H.; Melnikov, V.N. Regular black holes and black universes. *Gen. Relativ. Gravit.* **2007**, *39*, 973–987. [CrossRef]
12. Kardashev, N.S.; Novikov, I.D.; Shatskiy, A.A. Astrophysics of Wormholes. *Int. J. Mod. Phys. D* **2007**, *16*, 909–926. [CrossRef]
13. Dai, D.-C.; Stojkovic, D. Observing a wormhole. *Phys. Rev. D* **2019**, *100*, 083513. [CrossRef]
14. Nandi, K.K.; Zhang, Y.-Z.; Zakharov, A.V. Gravitational Lensing by Wormholes. *Phys. Rev. D* **2006**, *74*, 024020. [CrossRef]
15. Tsukamoto, N.; Harada, T. Light curves of light rays passing through a wormhole. *Phys. Rev. D* **2017**, *95*, 024030. [CrossRef]
16. Krasnikov, S.V. Schwarzschild-Like Wormholes as Accelerators. *Phys. Rev. D* **2018**, *98*, 104048. [CrossRef]
17. Mishra, A.; Chakraborty, S. On the trajectories of null and timelike geodesics in different wormhole geometries. *Eur. Phys. J.* **2018**, *78*, 374. [CrossRef]
18. Willenborg, F.; Grunau, S.; Kleihaus, B.; Kunz, J. Geodesic motion around traversable wormholes supported by a massless conformally-coupled scalar field. *Phys. Rev. D* **2018**, *97*, 124002. [CrossRef]
19. Stashko, O.S.; Zhdanov, V.I. Spherically symmetric configurations of General Relativity in presence of scalar field: Separation of test body circular orbits. *Gen. Relativ. Gravit.* **2018**, *50*, 105–114. [CrossRef]
20. Lee, J.; Koh, I. Galactic halos as boson stars. *Phys. Rev. D* **1996**, *53*, 2236–2239. [CrossRef]
21. Robles, V.H.; Matos, T. Flat central density profile and constant dark matter surface density in galaxies from scalar field dark matter. *Mon. Not. R. Astron. Soc.* **1996**, *422*, 282–289. [CrossRef]
22. Dokuchaev, V.I.; Eroshenko, Y.N. Weighing of the dark matter at the center of the Galaxy. *JETP Lett.* **2015**, *101*, 777–782. [CrossRef]

23. Cunha, P.V.P.; Herdeiro, C.A.R.; Radu, E. EHT Constraint on the Ultralight Scalar Hair of the M87 Supermassive Black Hole. *Universe* **2019**, *2*, 220. [CrossRef]
24. Matos, T.; Ureña-López, L.A. On the nature of dark matter. *Int. J. Mod. Phys. D* **2004**, *13*, 2287–2292. [CrossRef]
25. Ureña-López, L.A. Brief Review on Scalar Field Dark Matter Models. *Front. Astron. Space Sci.* **2019**, *6*, 47. [CrossRef]
26. Lamy, F.; Gourgoulhon, E.; Paumard, T.; Vincent, F.H. Imaging a non-singular rotating black hole at the center of the Galaxy. *Class. Quant. Grav.* **2018**, *35*, 115009. [CrossRef]
27. Dokuchaev, V.I.; Nazarova, N.O. Event Horizon Image within Black Hole Shadow. *J. Exp. Theor. Phys.* **2019**, *128*, 578–585. [CrossRef]
28. Bronnikov, K.A.; Korolyov, P.A. On wormholes with long throats and the stability problem. *Gravit. Cosmol.* **2017**, *23*, 273–279. [CrossRef]
29. Kratovitch, P.V.; Potashov, I.M.; Tchemarina, J.V.; Tsirulev, A.N. Topological geons with self-gravitating phantom scalar field. *J. Phys. Conf. Ser.* **2017**, *934*, 012047. [CrossRef]
30. Övgün, A. Deflection Angle of Photons through Dark Matter by Black Holes and Wormholes Using Gauss-Bonnet Theorem. *Universe* **2019**, *5*, 115. [CrossRef]
31. Bronnikov, K.A.; Chernakova, M.S. Charge black holes and unusual wormholes in scalar-tensor gravity. *Gravit. Cosmol.* **2007**, *13*, 51–55.
32. Bronnikov, K.A.; Sushkov, S.V. Trapped ghosts: A new class of wormholes. *Class. Quant. Grav.* **2010**, *27*, 095022. [CrossRef]
33. Bronnikov, K.A. Scalar Fields as Sources for Wormholes and Regular Black Holes. *Particles* **2018**, *1*, 56–81. [CrossRef]
34. Bronnikov, K.A.; Baleevskikh, K.A. On gravitational lensing by symmetric and asymmetric wormholes. *Gravit. Cosmol.* **2019**, *25*, 44–49. [CrossRef]
35. Hees, A.; Do, T.; Ghez, A.M.; Martinez, G.D.; Naoz, S.; Becklin, E.E.; Kosmo, K. Testing General Relativity with stellar orbits around the supermassive black hole in our Galactic center. *Phys. Rev. Lett.* **2017**, *118*, 211101. [CrossRef]
36. Bechmann, O.; Lechtenfeld, O. Exact black hole solution with selfinteracting scalar field. *Class. Quant. Gravit.* **1995**, *12*, 1473–1482. [CrossRef]
37. Bronnikov, K.A.; Shikin, G.N. Spherically symmetric scalar vacuum: No-go theorems, black holes and solitons. *Gravit. Cosmol.* **2002**, *8*, 107–116.
38. Nikonov, V.V.; Tchemarina, J.V.; Tsirulev, A.N. A two-parameter family of exact asymptotically flat solutions to the Einstein-scalar field equations. *Class. Quant. Gravit.* **2008**, *25*, 138001. [CrossRef]
39. Tchemarina, J.V.; Tsirulev, A.N. Spherically symmetric gravitating scalar fields. The inverse problem method and exact solutions. *Gravit. Cosmol.* **2009**, *15*, 94–96. [CrossRef]
40. Azreg-Aïnou, M. Selection criteria for two-parameter solutions to scalar-tensor gravity. *Gen. Relativ. Gravit.* **2010**, *42*, 1427–1456. [CrossRef]
41. Solovyev, D.A.; Tsirulev, A.N. General properties and exact models of static selfgravitating scalar field configurations. *Class. Quant. Gravit.* **2012**, *29*, 055013. [CrossRef]
42. Ellis, H.G. Ether flow through a drainhole: A particle model in general relativity. *J. Math. Phys.* **1973**, *14*, 104–118. [CrossRef]
43. Bronnikov, K.A. Scalar-tensor theory and scalar charge. *Acta Phys. Pol. B* **1973**, *4*, 251–266.
44. Ellis, H.G. Errata. *J. Math. Phys.* **1974**, *15*, 520. [CrossRef]
45. Ellis, H.G. The evolving, flowless drainhole: A nongravitating-particle model in general relativity theory. *Gen. Relativ. Gravit.* **1979**, *10*, 105–123. [CrossRef]
46. Chandrasekhar, S. *Mathematical Theory of Black Holes*; Oxford University Press: Oxford, UK, 1998.
47. Zakharov, A.F.; Borka, D.; Jovanović, V.B.; Jovanović, P. Constraints on $\mathbb{R}^n$ gravity from precession of orbits of S2-like stars. *Phys. Rev. D* **2012**, *85*, 124004.
48. Meyer, L.; Ghez, A.M.; Schödel, R.; Yelda, S.; Boehle, A.; Lu, J.R.; Matthews, K. The shortest known period star orbiting our galaxy's supermassive black hole. *Science* **2012**, *338*, 84–87. [CrossRef]

49. Potashov, I.M.; Tchemarina, J.V.; Tsirulev, A.N. Bound orbits near scalar field naked singularities. *Eur. Phys. J.* **2019**, *79*, 709. [CrossRef]
50. Potashov, I.M.; Tchemarina, J.V.; Tsirulev, A.N. Bound orbits near black holes with scalar hair. *J. Phys. Conf. Ser.* **2019**, *1390*, 012097. [CrossRef]